Designing Anthropomorphic Robot Hand With Active Dual-Mode Twisted String Actuation Mechanism and Tiny Tension Sensors

Seok Hwan Jeong, Kyung-Soo Kim, *Member, IEEE*, and Soohyun Kim

***Abstract*—In this letter, using the active dual-mode twisted string actuation (TSA) mechanism and tiny tension sensors on the tendon strings, an anthropomorphic robot hand is newly designed in a compact manner. Thanks to the active dual-mode TSA mechanism, which is a miniaturized transmission, the proposed robot hand dose has a wide range of operation in terms of the grasping force and speed. It experimentally produces maximally the fingertip force 31.3 N and minimally the closing time of 0.5 s in average. Also, tiny tension sensor with the dimension of 4.7 (width) $\times$ 4.0 (height) $\times$ 10.75 (length) mm is newly presented and embedded at the fingertips in order to measure the tension on the tendon strings, which would allow the grasping force control. The kinetic and kinematic analyses are performed and the performance is verified by experiments.**

***Index Terms*—Force and tactile sensing, multifingered hands, tendon/wire mechanism, twisted string actuation.**

I. Introduction

THERE have been continuous efforts on developing the anthropomorphic robot hands for various purposes either in the academy [1]–[4] and the industry [5]. Among many, considering a number of upper limb amputees [6], much attention has been paid to the prosthetic robot hands. For example, there exist commercially available robot hands such as iLimb (Touch Bionics, UK), Bebionic (RSL Steeper, UK), Vincent (Vincent System, Germany) and Michelangelo (Otto Bock, Germany) and etc. [5]. For these robot hands, electric motors with reduction gears are commonly adopted as actuators. However, in view point of mobility and compactness required for prosthetic devices, electrical motors have the generic disadvantage, i.e., much lower power density than that of the human muscles. Considering that a hand of an adult weighs about 400 gf and may generate a grasping force of maximally 400N with the flexion speed of 2,290 deg/s [7], the electrical motors with the reduction gears are too heavy and bulky to achieve the similar performance to the human hand.

To overcome the difficulty, several different types of actuator have been adopted for the robot hand design, such as the shape memory alloy [8], super-coiled polymers [9] the pneumatic [10] or the hydraulic actuators [11]. Theses may reduce the weight of the overall system or produce the large grasping power, however, suffer from their own drawbacks such as the slow response time, low power density, needs for compressors and etc.

More recently, new actuation mechanisms have been studied while adopting the electrical motors [12]–[15]. Force magnification drive in [12] and [13] belong to a kind of transmission systems which generate the large force or the high speed depending on the driving modes. It is noted that they effectively provide the different transmission ratios. However, their operating range is relatively small and, low power density and the complexity of the structure limit their application to the anthropomorphic robot hands. In [14], an adaptive joint mechanism was introduced for prosthetic hands, which effectively generates a large torque by passively increasing the moment arm at a finger joint when a large external force is exerted on the finger. However, it cannot switch the grip force automatically and loses power due to the passive mechanism. The power allocation mechanism in [15] shows 60% improvement in the fingertip force by utilizing the redundant degree of freedom. Overall, the aforementioned mechanisms contribute to the improvement in actuation to some extent. Nevertheless, they may not be complete enough to build up robot hands with anthropomorphic features.

In this paper, we aim at developing an anthropomorphic robot hand relying on the twisted string actuation (TSA) mechanism, a rotary-to-linear transmission, which produces a remarkably large contraction force by twisting a single or a pair of strings [16]–[19]. Since it does not use rigid gears, the TSA is mechanically simple and light. However, it suffer from the slow contraction speed. To resolve this issue, the passive dual-mode TSA was presented in [20], which allows the speed mode (with low contraction force) and the force mode (with low contraction speed) Later, as shown in Fig. 3, the speed and force modes can be easily switched by actively controlling a clutch motor [21], [22]. In fact, the so-called *active dual-mode* TSA mechanism allows the wide range of variable transmission ratio while maintaining light weight and the compactness. By employing

Manuscript received September 8, 2016; revised November 28, 2016; accepted December 21, 2016. Date of publication January 4, 2017; date of current version March 29, 2017. This paper was recommended for publication by Associate Editor P. Rocco and Editor R. Ozawa upon evaluation of the reviewers' comments. This work was supported by the Technology Innovation Program (10051330), which was funded by the Ministry of Trade, Industry and Energy (MI, South Korea) and the BK21 plus program through the National Research Foundation funded by the Ministry of Education of Korea.

The authors are with the Mechanical Engineering Department, Korea Advanced Institute of Science and Technology, Daejeon 305-701, South Korea (e-mail: astroidbelt@kaist.ac.kr; kyungsookim@kaist.ac.kr; soohyun@kaist.ac.kr).

Color versions of one or more of the figures in this paper are available online at http://ieeexplore.ieee.org.

Digital Object Identifier 10.1109/LRA.2017.2647800

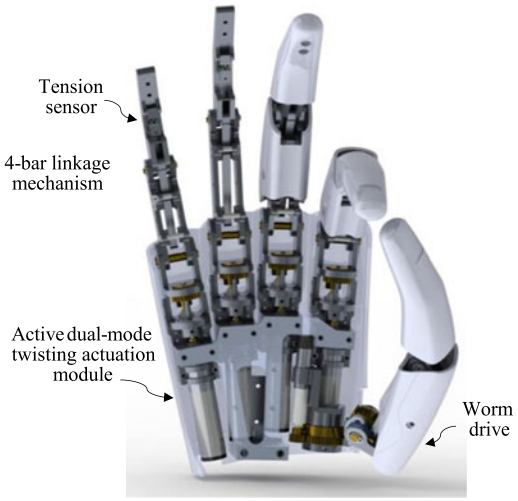

Fig. 1. Design of the developed anthropomorphic robot hand.

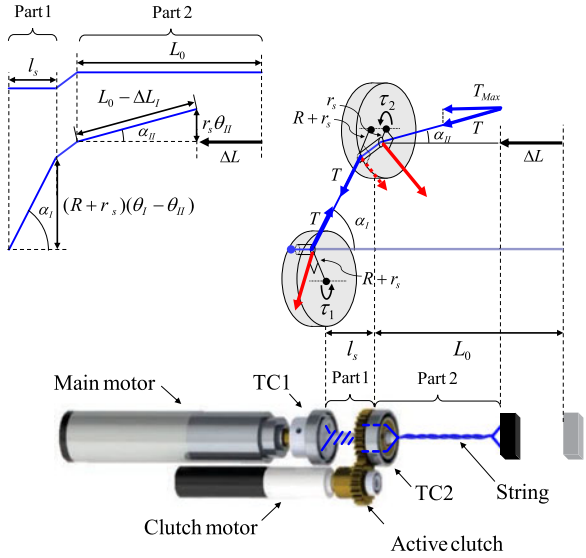

Fig. 2. Structure of the active dual-mode TSA.

the active dual-mode TSA mechanism, in this paper, we newly present an anthropomorphic robot hand of high performance, which may be ultimately used for prosthesis. Also, by embedding a new type of tension sensors, the tensions on the tendon string will be measured in the real time.

This paper is organized as follows. In Section II, the driving mechanism and design of the developed anthropomorphic robot hand are introduced. Section III is devoted to the analyses of kinetics and kinematics of the robot hand. In Section IV, grasping experiments with the developed robot hand are presented. Finally, the conclusion follows in Section V.

II. Design of Robot Hand

As shown in Fig. 1, the proposed robot hand consists of four fingers (i.e., index, middle, ring and little fingers) driven by four individual active dual-mode TSA modules, and a thumb actuated by two motors–one for adduction/abduction motions and the other for flexion/extension motions. Using the feature that the TSA mechanism produces the contraction force along with the twisted strings, the twisted strings play a role as a tendon for flexion of the finger. Also, to measure the tension on the twisted string (i.e., a tendon), a tiny tension sensor is placed at a fingertip and connected to the tendon, which is designed by using a small photo-interrupter. These four tension sensors would allow the real-time measurement and control of grasping force. It is noted that the extension of the finger is obtained by springs at the joints. In the following, the driving mechanism and the specific design of finger will be illustrated.

A. Revisit to Active Dual-Mode TSA Mechanism

In [20], a passive dual-mode with a single motor and a passive brake was introduce to generate a large flexion force or swift finger motion depending on the tension on the twisted string. However, it suffers from the complicated untying process and frictional loss of contraction force due to the passive brake. More recently, in [21], these problems have been solved by the active dual-mode TSA mechanism in which the passive brake is replaced with a small electric clutch motor. As shown in Fig. 2, the active dual-mode consists of a main motor, clutch motor, TC1 (twisted coupler 1), TC2 and strings. TC1 rotates with the angle, θ_I, by the main motor while TC2 does with the angle θ_{II} by the clutch motor. Observe that the relative angle between them may determine where the string are twisted (i.e., Part 1 or Part 2). Then it can be shown that the torques applied on TC1 and TC2 can be represented as follows:

$$\begin{aligned} \tau_1 &= (R + r_s) T \sin \alpha_I \\ \tau_2 &= (R + r_s) T \sin \alpha_I - r_s T \sin \alpha_{II} \end{aligned} \tag{1}$$

where R and r_s are the radii of the shaft in part 1 and the string, respectively, and T is the tension on the twisted strings, and, α_I and α_{II} are angles of inclination of the string in Part 1 and Part 2, respectively.

Then, the string tension, T and horizontal string tension, T_{Max} have the following relation: $T_{\mathrm{Max}} = T \cos \alpha_{II}$. It is noted that TC1 and TC2 are connected in a serial structure by the string, therefore, T is determined to be the minimum value of the tension generated by τ_1 and τ_2 from (1), having the following relation:

$$T_{\mathrm{Max}}(\alpha_I, \alpha_{II}) = \min \left[\left| \frac{\cos \alpha_{II}}{r \cdot \sin \alpha_I} \right| \tau_1, \frac{\tau_2}{\left| r_s \tan \alpha_{II} - r \frac{\sin \alpha_I}{\cos \alpha_{II}} \right|} \right] \tag{2}$$

It is noted that T_{Max} can be controlled with α_I and α_{II}, and they are also controlled with θ_I and θ_{II} as shown in Fig. 2.

According to (2), T_{Max} has a large value when $\alpha_I \approx 0$, that is, $\theta_I \approx \theta_{II}$, and this causes the strings to be twisted in part 2 and twisted around itself. We name this twisting mode as 'force mode.' In contrast, speedy contraction is generated when the strings are twisted around the shaft in part 1. We name this twisting mode as 'speed mode' as shown in Fig. 3. Then, from the geometric condition shown in Fig. 2, the contracted length

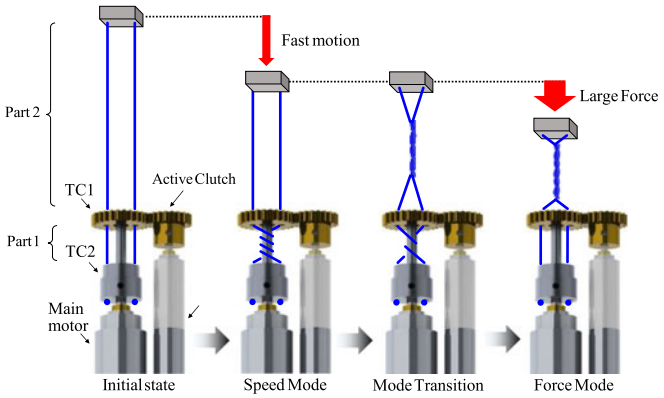

Fig. 3. Driving mechanism of the active dual-mode TSA.

TABLE I
SPECIFICATIONS OF THE DEVELOPED ROBOT HAND

Items	Specification
Robot hand Size	Average adult male hand size
Active dual-mode module size	69.2 mm × 19.5 × 15 mm
Weight	380 g
Number of actuators	Main motor: 4, Clutch motor: 4 Thumb motor: 2
Number of joints	11
Degree of freedoms	6
Average fingertip force	31.3 N (in force mode)
Closing time	0.5 s (in speed mode)
Main motor	Maxon motor (315170), 8 W, ϕ 10 64:1 gear, Nominal torque: 1.74 mNm
Clutch motor	Maxon motor (455020), 1.5 W, ϕ 6 57:1 gear, Nominal torque: 0.354 mNm
String radius, r_s	0.23 mm
Shaft radius, r	1 mm
Length of Shaft, l_s	7.7 mm
Initial length of part 2, L_0	89 mm (middle finger)
String material	Spectra fiber
Durability of tendon	Speed Mode: 28,500 cycle (200 gf) Force Mode: 3,005 cycle (2000 gf)

of the string ΔL is derived as follows:

$$\Delta L_I = \sqrt{{l_s}^2 + (R + r_s)^2(\theta_I - \theta_{II})^2} - l_s$$
$$\Delta L_{II} = (L_0 - \Delta L_I) - \sqrt{(L_0 - \Delta L_I)^2 - (r_s\theta_{II})^2}$$
$$\Delta L = \Delta L_I + \Delta L_{II} \tag{3}$$

ΔL_I and ΔL_{II} are contracted lengths in part 1 and part 2, respectively, and L_0 is the initial length of part 2.

Using the real parameters of the developed robot hand in Table I, the contraction force, T_{Max} corresponding to the contracted length, ΔL is plotted in each twisting mode, as shown in Fig. 4. It is noted that T_{Max} has different ranges in each twisting mode; therefore, the active dual-mode can play a role as a transmission by switching twisting modes.

As a result, a very compact and light transmission mechanism was implemented with the active dual-mode TSA. Therefore, we expect that this driving mechanism has many advantages in a compact robot system.

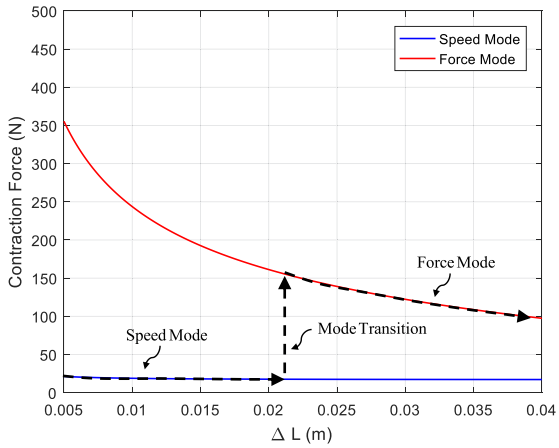

Fig. 4. Contraction force with respect to the contraction length.

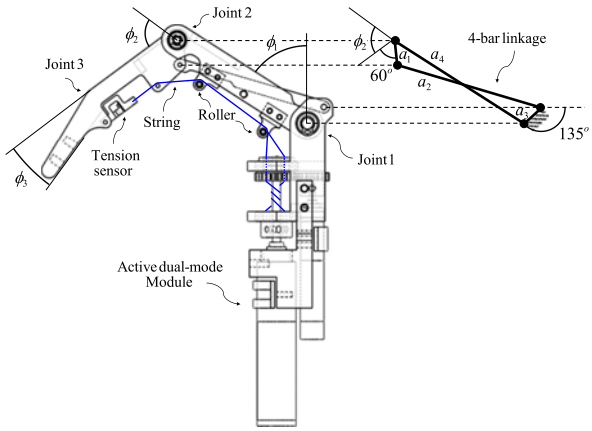

Fig. 5. Driving mechanism of the robot finger.

B. Finger Design

The fingers (i.e., index, middle, ring and little) of the developed robot hand are individually actuated by string contraction of the active dual-mode as shown in Fig. 5. The string is supported by rollers at each joints and connected to the tension sensor fixed at the fingertip. This driving structure may have an advantage for a compact design and is robust against external impact due to the self-compliance of the string. Meanwhile, because active-dual mode only provides contraction force to the string, a torsion spring is installed at joint 2 to provide reverse torque to the finger for extension motion.

The developed robot hand is designed to have one DOF per finger. Joint 1 and Joint 2 are mechanically coupled by 4-bar linkage, and Joint 3 is fixed for a simple and robust design. The structure of the 4-bar linkage is shown in Fig. 5, and the relation between joint 1 and joint 2 is as follows:

$$A = \sin(135^\circ - \phi_1), \quad B = \frac{a_4}{a_1} + \cos(135 - \phi_1)$$
$$C = \frac{a_4}{a_3}\cos(135 - \phi_1) + \frac{a_1^2 - a_2^2 + a_3^2 + a_4^2}{2a_1a_3}$$
$$\phi_2 = 2\tan^{-1}\left(\frac{A + \sqrt{A^2 + B^2 - C^2}}{B + C}\right) + 120^\circ \tag{4}$$

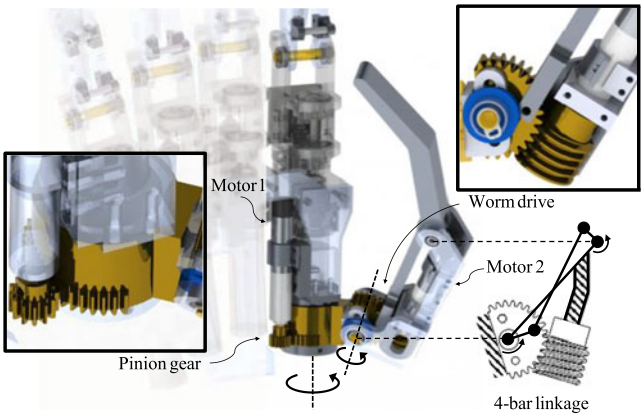

Fig. 6. Thumb design and driving mechanism.

where ϕ_1 and ϕ_2 are angle of joint 1 and joint 2, respectively, and, a_1, a_2, a_3 and a_4 is length of each link in 4-bar linkage.

The movement ratio between the ϕ_1 and ϕ_2, and the fixed joint angle 3, ϕ_3 are designed to be similar to the average human grasping posture [23].

C. Thumb Design

A Thumb of the human hand has 4 effective DOFs [24], accounting for up to 40% of the entire functionality of the hand [25]. Therefore, the design of the thumb is important for dexterous grasping. The developed robot hand has 2 DOFs for flexion/extension and abduction/adduction motion driven by 2 electric motors with worm drive and pinion gear, respectively as shown in Fig. 6.

The worm drive generates flexion/extension motion using non-back drivable feature, which is designed to withstand large grasping force from the active dual-mode. In addition, the rotation axis is tilted 30 degrees to the vertical direction for natural flexion/extension motion.

Abduction/adduction motion is obtained by a pair of pinion gears for generating various grasping posture (i.e., lateral grasp, power grasp or precision grasp).

D. Development of Tension Sensor

Many types of force sensor [26] such as tactile or pressure sensors have been developed for robot hands to obtain delicate grasping force control. However, for prosthetic devices, an increase in the number of force feedbacks to user exponentially reduces the force recognition rate and manipulability [27]. Moreover, these force sensors may be vulnerable to external impact, increase the cost of the system and need much wiring.

To resolve these problems, a miniature tension sensor using a photo-interrupter is newly designed in very compact, robust and cost-effective manner. The working principle of the sensor is shown in Fig. 7. Once an external load is applied to the elastic frame, deformation occurs, and the distance between the photo-interrupter and slit located on the light path is changed. This changes the amount of light entering the phototransistor, and the force can be indirectly estimated by measuring the output voltage of the phototransistor caused by the variance of light.

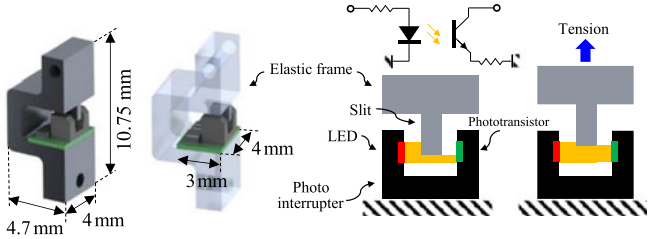

Fig. 7. Working principle of the photo-interrupter based force sensor.

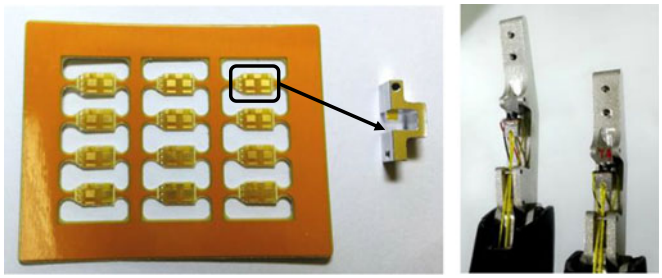

Fig. 8. Customized PCB for the photo-interrupter (left) and the tension sensor embedded in the robotic fingertip (right).

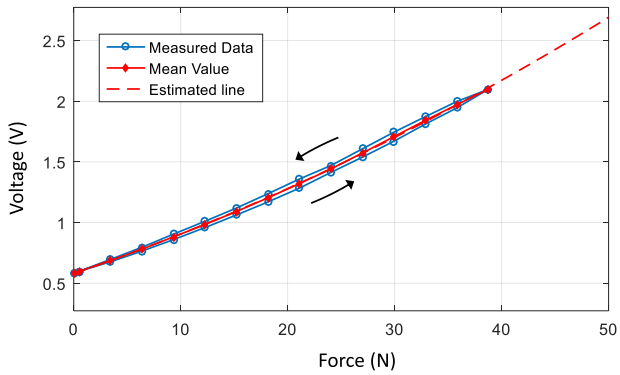

Fig. 9. Relation between force-input and voltage-output of tension sensor.

Although photo-interrupter based force sensors have already been developed in [28], [29], these are too large in size to be embedded in compact systems such as robotic fingers. Therefore, the developed sensor is designed in a compact manner to be embedded in the fingertip as shown in Fig. 8. A commercial ultraminiature photo-interrupter (rpi-0128, Rohm, Japan) is used, and customized printed circuit board (PCB) for the photo-interrupter is designed for the power supply and signal acquisition. The sensor is designed to measure the tension of the string and be a modular type which can be easily installed in other tendon based application. The volume and weight of the sensor are 4.7 mm $\times$ 4 mm $\times$ 10.75 mm and 0.25 g, and the capacity is about 100 N. In addition, it is made of aluminum 7075 (AL7075) to minimize hysteresis characteristic. Experiment result for the force-input and voltage-output is shown in Fig. 9. Based on the experimental result, linear regression is used for the force estimation. The hysteresis of the sensor is under 4.5% which is relatively larger than 1% hysteresis of a compact size commercial force sensor (SlimLine sensor, KISTLER,

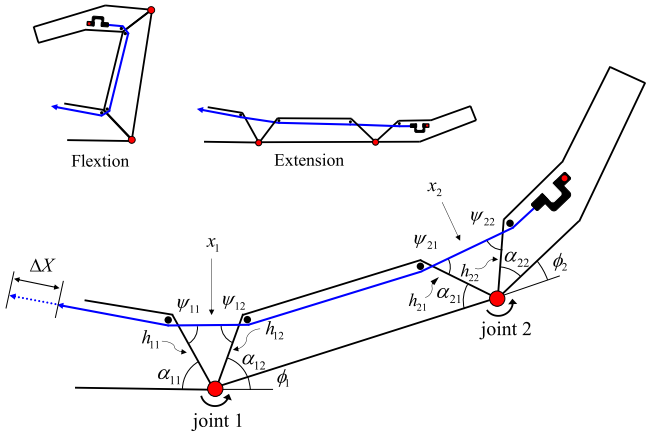

Fig. 10. Geometry of the developed robot finger.

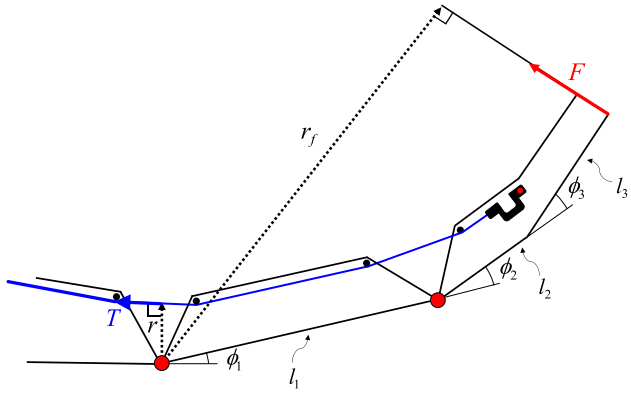

Fig. 11. Relation between tension and fingertip force.

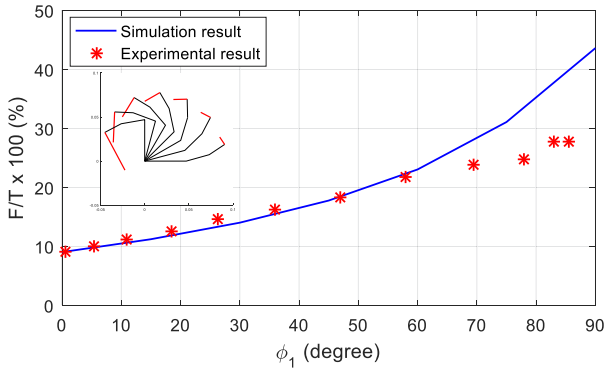

Fig. 12. Conversion rate from the string tension to the fingertip force.

Swiss) with a volume of 4 mm × 14 mm × 14 mm; however, it is a reasonable value considering the low cost and miniaturized design.

III. Analysis of the Robot Hand

Kinematics and kinetics for a tendon based manipulator were analyzed in [20], [22]. In this chapter, mathematic models for the developed robot hand are derived. The bending angles of each joint by the contraction of the string and the relation between the fingertip force, string tension and joint angles are derived. Furthermore, a feed forward neural network model is introduced for estimation of the contracted length of the twisted string having highly non-linear feature.

A. Kinematics

Fig. 10 is a simple diagram of the developed robotic finger. ΔX is the contraction length of the string and h, α, ψ are geometric parameters consisting the finger as shown in Fig. 10. Then, the relation between ΔX and kth joint angle ϕ_k is as follows:

$$\begin{aligned}\Delta X &= X_O - X = \Delta x_1 + \Delta x_2 \\ &= \sum_{j=1}^{2} \sqrt{h_{j1}^2 + h_{j2}^2 + 2h_{j1}h_{j2}\cos(\alpha_{n1} + \alpha_{n2})} \\ &\quad - \sum_{k=1}^{2} \sqrt{h_{k1}^2 + h_{k2}^2 + 2h_{k1}h_{k2}\cos(\alpha_{k1} + \alpha_{k2} + \phi_k)}\end{aligned} \tag{5}$$

Using this equation, the grasping angle of the finger can be adjusted by controlling the contracted length of the string. In the case of the developed robot hand, ΔX should be 32.35 mm (for the middle finger) for full flexion motion from full extension motion as shown in Fig. 10.

B. Kinetics

Tension T applied to the string generates torque at each joint, and it is converted to fingertip force F as shown in Fig. 11. Then, the relation between tension T and fingertip force F is expressed by the moment equilibrium equation:

$$\vec{r} \times \vec{T} = \vec{r}_f \times \vec{F}$$

$$F = \frac{h_{12}\sin\psi_{12}T}{l_1\cos(\phi_2 + \phi_3) + l_2\cos(\phi_3) + l_3} \tag{6}$$

As a result, the fingertip force F can be estimated from joint angle ϕ_k, string tension T measured by the tension sensor. Fig. 12 shows that the conversion rate from T to F with changing joint 1 angle ϕ_1 and an experimental result. The simulation result shows that the finger generates a small fingertip force with a large moment arm r_f when the finger is extended, but generates a large fingertip force with a small moment arm r_f when it makes a flexion motion under the same string tension. The average conversion rate from flexion to extension is approximately 21.4%. The experimental result shows that the force estimation of the fingertip is very accurate at less-than-60-degree joint angle; however, error is increased after that angle. Because excessive flexion posture increases friction between the string and rollers, tension is not evenly distributed on the string. This reduces the conversion rate and it is less than the simulation result. However, this is not a big problem because most grasping motion occurs under 60 degrees.

On the contrary, the external force applied to the fingertip is converted to string tension and it is amplified approximately

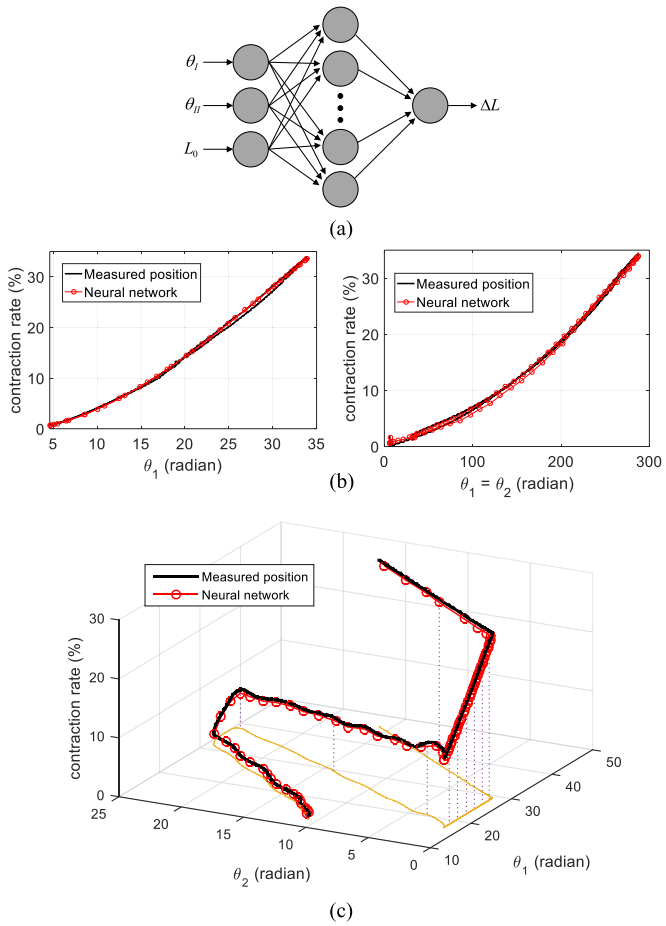

Fig. 13. (a) Feed forward neural network structure. (b) Estimation of the contracted length in speed mode (right) and force mode (left). (c) Estimation of the contracted length in mixed twisting modes.

5 folds; therefore, it may have 5-fold increase in resolution for tension.

C. Estimation of Contraction Length

For the precise grasping motion control, exact model for estimating the contracted length of the string is required. The contraction model of TSA has been studied in [16]–[19], and it shows good estimation result within a certain contraction rate. However, it is difficult to obtain accurate estimation results in more than about 10% contraction rate due to high nonlinearity of the TSA.

Therefore, we can conclude that additional position sensors are essential for accurate contraction length estimation. Especially, because the active dual-mode has one more DOF than general TSA, model based position estimation is more difficult.

To resolve this difficulty, a feed forward neural network (FNN) model is introduced to estimate the exact contracted length of the string without additional position sensors. Fig. 13(a) is a structure of FNN. θ_I, θ_{II} and L_0 are used as inputs of FNN, and the total contracted length of the string ΔL is designed as an output of FNN. To obtain various ground truth data, 35% contraction motions were repeated for 5 minutes while changing the ratio between speed and force mode at

Fig. 14. The developed robot hand and various grasping posture.

regular intervals. All input data are measured with hall sensors of motor and position sensor with 1 kHz sampling rate. After that, neural network toolbox (MATLAB 2016a) is used for training FNN having one hidden layer consisting of 20 nodes. As a result, the trained FNN shows 2.52% and 4.80% mean percentage errors in the speed mode and force mode, respectively, within 0–30% contraction rate as shown in Fig. 13(b). Moreover, the FNN has under 3% error rate in mixed twisting modes as shown in Fig. 13(c). This result shows that FNN can guarantee the accuracy of position in a wide contraction rate without additional position sensors.

However, the tension data of the string are excluded from the input of FNN for simple acquisition of training data. It will be possible to build a more exact FNN structure by considering the elongation of string under various tension later on.

IV. Experiments

Fig. 14 is a developed anthropomorphic robot hand using active dual-mode and tiny tension sensor, and shows various grasping posture. In this chapter, the experimental results of the robot hand and tension sensor are introduced. All experiments were conducted under nominal torque condition of the motor. The major specifications are summarized in Table I.

A. Grasping Force and Speed

The robot hand using active dual-mode can operate in speed mode or force mode, respectively, depending on the grasping situation.

In experiment 1, we measured the grasping time from full extension motion ($\phi_1 = 0$) to full flexion motion ($\phi_1 = 90°$). In the experimental results, it takes 0.5 s and 3.3 s in speed mode and force mode, respectively, as shown in Fig. 15(a). 0.5 s

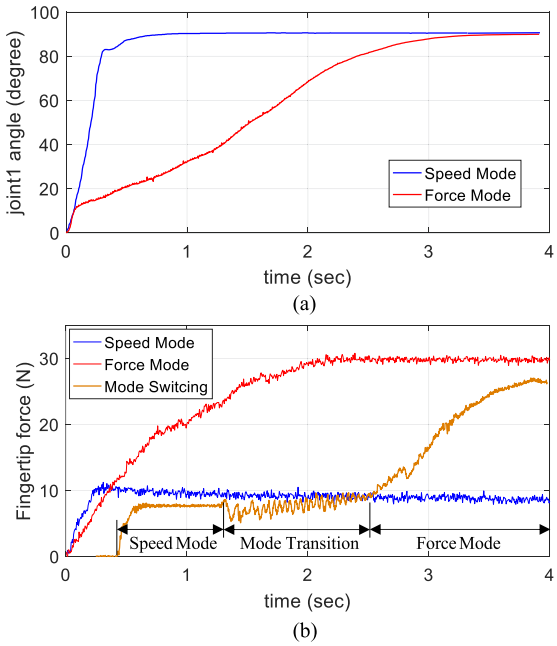

Fig. 15. Performance of the robot hand in speed mode (blue), force mode (red) and mode switching (yellow) (a) Joint angle (b) Fingertip force.

of grasping time is short enough than 0.8 s which has been suggested as sufficient closing time for the prosthetic hand in [30], and it is fast enough to interact with the external environment.

In experiment 2, we measured the normal force of the fingertip applied to the load cell. As shown in Fig. 15(b), the maximum measured forces are 11.25 N and 30.8 N in speed mode and force mode, respectively, once the joint 1 angle ϕ_1 is 45 degrees. Force mode can generate a fingertip force from 15.7 N to 48.2 N depending on the finger posture, and the average is 31.3 N. Therefore, grasping force of the developed hand can reach about 128 N and sufficiently exceeds 45 N which is the minimum grasping force suggested in [30], if the robot hand uses all fingers.

A mode switching experiment was also conducted. First, the finger generates a fast flexion motion in speed mode, keeping contact with the object with a small force. Subsequently, the grasping mode is switched from speed mode to force mode by the mode transition process, and the finger makes large contact force with the object in force mode. As shown in Fig. 15(b), the mode switching is successfully implemented. However, there are small perturbations during mode transition; this may cause unstable grip. However, the perturbations are always larger than 0 N and the average value remains almost constant. Therefore, the finger can keep contact with the object without dropping during the mode transition. In addition, because most precision grips are performed in speed mode, the perturbations may not significantly affect the grasping performance.

B. Force Control Using the Tension Sensor

In experiment 3, we conducted grasping force control with the developed tension sensor. Tension measured from the tension

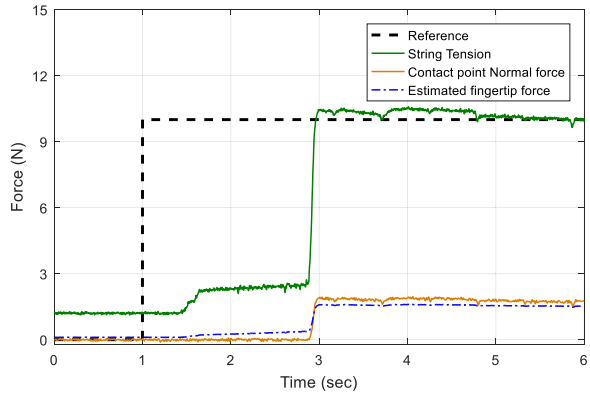

Fig. 16. Tension of the string (green) measured by the tension sensor, fingertip force (yellow) from the load cell and estimated fingertip force (blue).

sensor is used for proportional-integral (PI) control to maintain 10 N of tension, and the corresponding fingertip force is measured by the load cell at the same time. The experimental result shows that the tension tracks the reference correctly as shown in Fig. 16, and the fingertip applies force to the load cell, maintaining a fixed ratio with the tension. In addition, as shown by the blue dotted line of Fig. 16, the fingertip force calculated by (6) accurately estimates real value within 10% error rate.

C. Durability of the String

Thanks to the use of spectra fiber string (Honeywell, USA), which is ultrahigh molecular weight polyethylene, the string has very high durability and tensile strength to withstand 55 kgf with radius of 0.23 mm. From the durability test, the lifetime of the string is 28,500 and 3,005 cycles under 200 gf and 2000 gf tension in speed and force mode, respectively.

V. Conclusion

In this paper, an anthropomorphic robot hand is designed by using an active dual-mode TSA mechanism and tiny tension sensor. The developed hand has a wide operating area in terms of the grasping force and speed. The robot hand produces maximally the fingertip force of 31.3 N and minimally the closing time of 0.5 s in force mode and speed mode, respectively. It may perform various tasks in daily life by switching driving modes depending on situation. Furthermore, because the total weight of the developed robot hand was only 380 g, (i.e., lower than the human hand weight of 400 g), it is suitable for use as a prosthetic device.

By using the photo-interrupter-based force-sensing mechanism, the force sensor can be miniaturized and embedded in the fingertip of the robot hand. We conducted force feedback grasping control using the developed tension sensor.

FNN is used for estimation of the contracted length of twisted string for precise grasping motion control without additional position sensors. It shows better estimation results compared to estimations based on existing models.

Future work will focus on the grasping control algorithm, stability in the mode change process and application for the prosthetic hand using bio signals.

REFERENCES

[1] S. A. Dalley, T. E. Wiste, T. J. Withrow, and M. Goldfarb, "Design of a multifunctional anthropomorphic prosthetic hand with extrinsic actuation," *IEEE/ASME Trans. Mechatronics*, vol. 14, no. 6, pp. 699–706, Dec. 2009.

[2] M. Hioki *et al.*, "Design and control of electromyogram prosthetic hand with high grasping force," in *Proc. 2011 IEEE Int. Conf. Robot. Biomimetics*, 2011, pp. 1128–1133.

[3] A. Akhtar *et al.*, "A low-cost, open-source, compliant hand for enabling sensorimotor control for people with transradial amputations," in *Proc. 2016 38th Annu. Int. Conf. IEEE Eng. Med. Biol. Soc.*, 2016, pp. 4642–4645.

[4] C.-H. Xiong, W.-R. Chen, B.-Y. Sun, M.-J. Liu, S.-G. Yue, and W.-B. Chen, "Design and implementation of an anthropomorphic hand for replicating human grasping functions," *IEEE Trans. Robot.*, vol. 32, no. 3, pp. 652–671, Jun. 2016.

[5] J. T. Belter and J. L. Segil, "Mechanical design and performance specifications of anthropomorphic prosthetic hands: A review," *J. Rehabil. Res. Develop.*, vol. 50, p. 599–618, 2013.

[6] K. Ziegler-Graham, E. J. MacKenzie, P. L. Ephraim, T. G. Travison, and R. Brookmeyer, "Estimating the prevalence of limb loss in the United States: 2005 to 2050," *Arch. Phys. Med. Rehabil.*, vol. 89, pp. 422–429, 2008.

[7] C. Heckathorne, "Components for adult externally powered systems," *Atlas Limb Prosthetics, Surg,, Prosthetic, Rehabil. Principles*, vol. 2, pp. 151–174, 1992.

[8] K. Andrianesis and A. Tzes, "Development and control of a multifunctional prosthetic hand with shape memory alloy actuators," *J. Intell. Robot. Syst.*, vol. 78, pp. 257–289, 2015.

[9] M. C. Yip and G. Niemeyer, "High-performance robotic muscles from conductive nylon sewing thread," in *Proc. 2015 IEEE Int. Conf. Robot. Autom.*, 2015, pp. 2313–2318.

[10] R. Deimel and O. Brock, "A compliant hand based on a novel pneumatic actuator," in *Proc. 2013 IEEE Int. Conf. Robot. Autom.*, 2013, pp. 2047–2053.

[11] S. Guitao, S. Junpeng, D. Xiang, and W. Xiaojing, "Hydraulic robot force control based on environment parameters adaptive estimation," *J. Huazhong Univ. Sci. Technol. Natural Sci. Ed.*, vol. 4, pp. 26–31, 2015.

[12] T. Takaki and T. Omata, "High-performance anthropomorphic robot hand with grasping-force-magnification mechanism," *IEEE/ASME Trans. Mechatronics*, vol. 16, no. 3, pp. 583–591, Jun. 2011.

[13] T. Takayama, T. Yamana, and T. Omata, "Three-fingered eight-DOF hand that exerts 100-N grasping force with force-magnification drive," *IEEE/ASME Trans. Mechatronics*, vol. 17, no. 2, pp. 218–227, Apr. 2012.

[14] A. Hernandez Arieta, R. Katoh, H. Yokoi, and Y. Wenwei, "Development of a multi-DOF electromyography prosthetic system using the adaptive joint mechanism," *Appl. Bionics Biomech.*, vol. 3, pp. 101–111, 2006.

[15] T. Seki, T. Nakamura, R. Kato, S. Morishita, and H. Yokoi, "Development of five-finger multi-DoF myoelectric hands with a power allocation mechanism," in *Proc. 2013 IEEE Int. Conf. Robot. Autom.*, 2013, pp. 2054–2059.

[16] M. Shoham, "Twisting wire actuator," *J. Mech. Des.*, vol. 127, pp. 441–445, 2005.

[17] T. Würtz, C. May, B. Holz, C. Natale, G. Palli, and C. Melchiorri, "The twisted string actuation system: Modeling and control," in *Proc. 2010 IEEE/ASME Int. Conf. Adv. Intell. Mechatron.*, 2010, pp. 1215–1220.

[18] T. Sonoda and I. Godler, "Position and force control of a robotic finger with twisted strings actuation," in *Proc. 2011 IEEE/ASME Int. Conf. Adv. Intell. Mechatron.*, 2011, pp. 611–616.

[19] I. Gaponov, D. Popov, and J.-H. Ryu, "Twisted string actuation systems: A study of the mathematical model and a comparison of twisted strings," *IEEE/ASME Trans. Mechatronics*, vol. 19, no. 4, pp. 1331–1342, Aug. 2014.

[20] Y. J. Shin, H. J. Lee, K.-S. Kim, and S. Kim, "A robot finger design using a dual-mode twisting mechanism to achieve high-speed motion and large grasping force," *IEEE Trans. Robot.*, vol. 28, no. 6, pp. 1398–1405, Dec. 2012.

[21] S. H. Jeong, Y. J. Shin, K.-S. Kim, and S. Kim, "Dual-mode twisting actuation mechanism with an active clutch for active mode-change and simple relaxation process," in *Proc. IEEE/RSJ Int. Conf. Intell. Robots Syst.*, 2015, pp. 5832–5837.

[22] S. H. Jeong, K.-S. Kim, and S. Kim, "Development of a robotic finger with an active dual-mode twisting actuation and a miniature tendon tension sensor," in *Proc. 2016 IEEE Int. Conf. Adv. Intell. Mechatron.*, 2016, pp. 1–6.

[23] J. N. Ingram, K. P. Körding, I. S. Howard, and D. M. Wolpert, "The statistics of natural hand movements," *Exp. Brain Res.*, vol. 188, pp. 223–236, 2008.

[24] L. Cheze, R. Dumas, J.-J. Comtet, C. Rumelhart, and M. Fayet, "Determination of the number of degrees of freedom of the trapeziometacarpal joint—An in vitro study," *IRBM*, vol. 33, pp. 272–277, 2012.

[25] E. Ouellette, J. McAuliffe, and R. Caneiro, "Partial-hand amputations: Surgical principles," in *Atlas of Limb Prosthetics: Surgical, Prosthetic, and Rehabilitation Principles*. St. Louis, MO, USA: Mosby, 1992.

[26] H. Yousef, M. Boukallel, and K. Althoefer, "Tactile sensing for dexterous in-hand manipulation in robotics—A review," *Sens. Actuators A, Phys.*, vol. 167, pp. 171–187, 2011.

[27] D. Zhang, H. Xu, P. B. Shull, J. Liu, and X. Zhu, "Somatotopical feedback versus non-somatotopical feedback for phantom digit sensation on amputees using electrotactile stimulation," *J. Neuroeng. Rehabil.*, vol. 12, pp. 1–11, 2015.

[28] D. Tsetserukou, R. Tadakuma, H. Kajimoto, and S. Tachi, "Optical torque sensors for implementation of local impedance control of the arm of humanoid robot," in *Proc. IEEE Int. Conf. Robot. Autom.*, 2006, pp. 1674–1679.

[29] J.-C. Kim, K.-S. Kim, and S. Kim, "Wearable sensor system including optical 3-axis GRF sensor for joint torque estimation in real-time gait analysis," in *Proc. 2014 IEEE/ASME Int. Conf. Adv. Intell. Mechatron.*, 2014, pp. 112–117.

[30] R. Vinet, N. Beaudry, and G. Drouin, "Design methodology for a multifunctional hand prosthesis," *J. Rehabil. Res. Develop.*, vol. 32, pp. 316–324, 1995.